Journal of Materials Chemistry C

ROYAL SOCIETY OF CHEMISTRY

PAPER

View Article Online
View Journal | View Issue

Cite this: J. Mater. Chem. C, 2022, 10, 13954

Chiral nanostructures derived from europium(III) complexes for enhanced circularly polarised luminescence and antibacterial activity†

Betsy Marydasan,[ab] Karthika Suryaletha,[c] Amrutha Manoj Lena,[a] Alida Sachin,[a] Tsuyoshi Kawai,[d] Sabu Thomas[c] and Jatish Kumar*[a]

Nanomaterials that exhibit a multitude of properties are gaining vast attention in recent years. Minimising the material consumption and simplifying the manifold synthetic routes adopted for the preparation of diverse molecules and materials are the major advantages offered by such materials. Herein, we report the synthesis of a series of optically active heterobimetallic Eu(III) complexes with the general formula $M^{+}[Eu((+)-tfac)_4]^{-}$ (M = Cs, Rb, K, Na) using chiral 3-trifluoroacetylcamphorate as the ligand. The metal coordinated complex forms an interesting one-dimensional polymer crystal which further extends to arrays resulting in a coordination network structure. The synthesized complexes exhibited high circularly polarized luminescence. The optical activity was dependent on the size of the alkali metal cation and was found to increase with the increase in the size of the ion. The caesium derivative of the complex exhibited a remarkably high luminescence dissymmetry value and a high luminescence quantum yield. The complexes undergo self-assembly in suitably selected solvents forming chiral nanostructures. The aggregated structures of all the four derivatives showed high chiral luminescence both in the solution state and solid films. In addition to chiral luminescence, the complexes exhibited promising antibacterial activity towards multidrug resistant bacterial strains *Staphylococcus aureus* and *Enterococcus faecalis*, microbes that form the root cause of consequential co-morbidities and mortality to humankind. Moreover, the high luminescence quantum yield exhibited by the complexes shows promise towards bioimaging applications. The facile approach opens new avenues for finding potential applications for the lanthanide based nanosystems, both as efficient chiral luminescent materials and as effective antibacterial agents.

Received 26th May 2022,
Accepted 16th June 2022

DOI: 10.1039/d2tc02193e

rsc.li/materials-c

Introduction

Chiral optics has gained immense attention in recent years due to its potential applications in interdisciplinary fields like photonic displays, anti-counterfeit tags, quantum information storage, and biological sensing.[1,2] While chiral absorption is extensively reported using circular dichroism (CD),[3,4] the differential emission of left and right circularly polarized light termed as circularly polarized luminescence (CPL) is relatively new.[5,6] The last decade has seen a surge in the amount of work devoted to the development of CPL active materials, not only due to the wide applicability of CPL, but also due to the vast structural information it generates about the chiral molecule and its environment in the excited state.[6–8] Any future application of CPL active material is majorly governed by two important factors: (i) high luminescence anisotropy factor (g_{lum}) and (ii) the ability of the material to exhibit reliable properties in solution and solid state.[9–11] The g_{lum} measures the extent of chiral dissymmetry in emission, and can be theoretically denoted as $g_{lum} = 4(\mu_{ij}\cdot m_{ij})/(|\mu_{ij}|^2 + |m_{ij}|^2)$, where m and μ are the magnetic and electric transition dipole moment vectors, respectively.[11] It is evident from the equation that molecules exhibiting magnetic dipole allowed transitions are favourable candidates that can generate high luminescence anisotropy. In this context, special focus has been on lanthanide systems owing to their parity allowed magnetic dipole transition within

[a] Department of Chemistry, Indian Institute of Science Education and Research (IISER) Tirupati, Tirupati 517507, India. E-mail: jatish@iisertirupati.ac.in
[b] Department of Chemistry, Government Arts College, Thiruvananthapuram, Kerala 695014, India
[c] Cholera and Biofilm Research laboratory, Rajiv Gandhi Centre for Biotechnology (National Institute under the Dept. of Biotechnology, Govt. of India), Trivandrum, Kerala, India
[d] Graduate School of Materials Science, Nara Institute of Science and Technology, Ikoma, Nara 630-0192, Japan

† Electronic supplementary information (ESI) available. CCDC 2122503. For ESI and crystallographic data in CIF or other electronic format see DOI: https://doi.org/10.1039/d2tc02193e

the f-orbitals.[12–15] Moreover, sharp emission bands, reasonably good luminescence quantum yield, and high luminescence lifetime label them as ideal CPL active materials.[16–19] Research in this direction has revealed that coordination of the chiral chromophores to metal centres can be an effective design strategy for the enhancement of the anisotropic factor.[20–23] Kaizaki and coworkers have observed exceptionally large CPL in Eu(III) complexes containing chiral β-diketonate ligands with a camphor framework.[24,25] Furthermore, the assembly of these complexes to form chiral nanostructures has gained augmented attention due to their enhanced performance, in terms of both luminescence dissymmetry and quantum yield.[20] While the self-assembly of molecules forming nanostructures with enhanced g_{lum} has been extensively investigated in organic luminophores,[11,26] such studies in lanthanide-based complexes are scarce. Herein, we focus on the development of Eu(III) complexes and their nanostructures that exhibit high chiral luminescence in solution as well as solid state.

Recently, research focus has diverted attention towards the development of active materials capable of exhibiting a multitude of functional properties.[27–29] This will minimize the material consumption and simplify the otherwise manifold synthetic routes adopted for the preparation of diverse molecules and materials.[30] In this regard, the use of optically active molecules in the biomedical field is an interesting development.[31] In this era of emerging antibiotic resistance, it is highly relevant that we design novel drug combinations that work effectively against rising bacterial infections.[32,33] The World Health Organization (WHO) has enlisted a top priority pathogen list, which emphasizes the undeniable need for the development of a new class of antibiotics to tackle this systemic problem.[34] Despite the vast potential of lanthanide complexes as antimicrobial agents, studies in this direction have gained very little attention.[35] Realising their relevance under the current circumstances, we have identified promising candidate molecules that show activity against the high priority Gram positive nosocomial pathogens, multidrug resistant *Staphylococcus aureus* and *Enterococcus faecalis*, microbes that form the root cause of consequential co-morbidities and mortality to humankind.[36,37] We have synthesized a set of chiral nanostructures from heterobimetallic Eu(III) complexes with 3-trifluoroacetyl-(+)-camphorate (tfac) as a chiral ligand, that can function as effective antibacterial agents. Low toxicity along with enduring luminescence makes these complexes promising candidates for biomedical applications. Moreover, they exhibit high CPL activity, opening new avenues for the use of CPL active materials in biomedical research (Fig. 1).

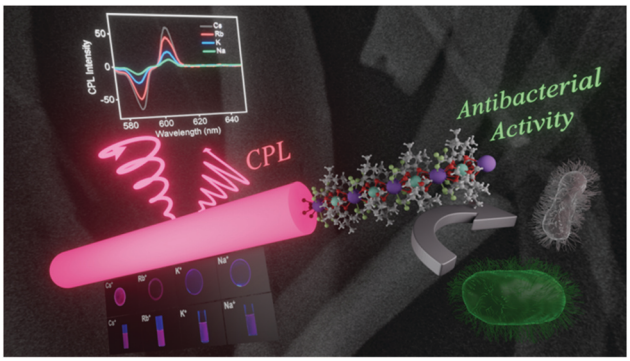

Fig. 1 Scheme illustrating the use of the Eu(III) trifluoroacetylcamphorate complex and the corresponding nanomaterials as both (i) CPL active materials and (ii) antibacterial agents.

Jatish Kumar

Jatish Kumar obtained his PhD in Chemistry from the CSIR-National Institute for Interdisciplinary Science and Technology (NIIST), Trivandrum, India. After completion of his PhD, he worked initially as a JSPS postdoctoral fellow and later as an assistant professor at the Nara Institute of Science and Technology (NAIST), Nara, Japan. Later he moved as a Marie Curie postdoctoral fellow to CIC biomaGUNE in San Sebastian, Spain. He joined the Indian Institute of Science Education and Research (IISER) Tirupati, India, as an Assistant Professor in December 2018. His research interests are in the field of nanoscale chirality, photochemistry and assembly of nanomaterials.

Experimental section

Materials

Chlorides and sulphates of caesium(I), rubidium(I), potassium(I), and sodium(I) were obtained from Tokyo Chemical Industry Co., Ltd (TCI), India. The complex europium(III) tris-[3-(trifluoromethylhydroxymethylene)-(+)-camphorate] was purchased from Sigma-Aldrich chemicals Private Limited, India. Reagents and solvents were also purchased from the above mentioned commercial sources.

Synthesis of the complex

The alkali metal tetrakis 3-trifluoroacetyl-(+)-camphorato europium(III) complex was synthesized from tris(3-trifluoroacetyl-(+)-camphorato)europium(III) (Eu((+)–tfac)$_3$) by the reaction with 10 equivalents of the metal salt (chloride/sulphate) in a chloroform–water mixture for 3 h at room temperature. The schematic representation of the synthesis and the structure of $M^+[Eu((+)\text{-tfac})_4]^-$ is shown in Fig. S1 (ESI†). The synthesized Eu(III) complexes were crystallised in an ethyl acetate–hexane solvent mixture. The structure of the bimetallic complex $Cs^+[Eu((+)tfac)_4]^-$ was investigated using single-crystal X-ray analysis.

Sample preparation for analysis

All photophysical and chiroptical measurements were carried out in chloroform and DMSO solutions. Sonication was done to achieve maximum solvation. For solid-state studies, samples were prepared by dissolving 0.8 g of PMMA in chloroform

followed by the addition of the samples dissolved in chloroform to reach a total volume of 10 ml. The solution was then heated at 40 °C for 40 min and allowed to cool to room temperature. A part of the solution was coated on quartz plates and used for photophysical and chiroptical studies. The composite polymer solution was transferred to a Petri dish and allowed to dry to obtain free standing films after complete evaporation of the solvent.

Characterization

All photophysical and chiroptical studies were done in 2 mM chloroform and DMSO solution unless stated otherwise. UV-vis spectra were collected on a Cary 5000 high-performance UV-vis and NIR spectrophotometer. Photoluminescence measurements were performed on JASCO FP-8500 equipped with a 150 W xenon lamp with medium sensitivity. CD spectra were collected on a JASCO J-1500 Series spectrometer with a 150 W xenon lamp as the light source. The CPL studies were performed on JASCO CPL-300 with a 150 W xenon arc lamp. Single crystal XRD measurements were made on a Rigaku R-AXIS RAPID diffractometer using filtered Mo-Kα radiation. Luminescence lifetime was measured using the Edinburg FLS-1000 fluorescence spectrometer. Absolute quantum yield measurements were done using the integrating sphere in an Edinburg FLS-1000 instrument.

Antibacterial activity

The complexes were tested for antibacterial activity against a set of Gram positive (*Staphylococcus aureus* ATCC 25923, methicillin resistant *Staphylococcus aureus* (MRSA) 145, MRSA 108, *S. aureus* 470, *Enterococcus faecalis* ATCC 29212, *E. faecalis* SK460) and Gram negative pathogens (*Escherichia coli* ATCC 25922, *Pseudomonas aeruginosa* ATCC 27853, *Salmonella typhi*, and *Vibrio cholerae* MCV09).

Broth microdilution assay was performed to check the antibacterial activity of compounds at 100, 75, 50, 35 and 25 μM concentrations. The culture inoculum with DMSO was used as the negative control for each strain. After 24 h incubation, the growth inhibition was studied by monitoring the absorbance at 600 nm in a Microplate Absorbance Reader (iMark™, BioRad, US).

Broth microdilution assay

To perform the broth microdilution assay, overnight culture of each pathogen was grown in Muller Hinton broth (Himedia, India) medium and was diluted to 0.1 O.D. at 600 nm. The compounds were dissolved in DMSO and added to the above diluted bacterial culture at different concentrations ranging from 100, 75, 50, 35 and 25 μM. Further, the broth microdilution assay was performed in 96 well microliter plates (Nunc, Denmark). The culture inoculum with DMSO was used as the negative control for each strain. After 24 h incubation, the growth inhibition was studied by monitoring the absorbance at 600 nm in a Microplate Absorbance Reader (iMark™, BioRad, US).

The percentage of bacterial inhibition was calculated using the following equation:

$$\%\ \text{inhibition} = [1 - (X_{A600}/C_{A600})] \times 100$$

where X_{A600} and C_{A600} represent the absorbance of the compound treated bacterial culture and the control culture at 600 nm, respectively.

The minimum inhibitory concentration (MIC) of $Cs^+[Eu((+)\text{–tfac})_4]^-$ was determined against susceptible pathogens using the microdilution method as per the guidelines of the Clinical and Laboratory Standards Institute against susceptible pathogens (CLSI, 2012).

Hemolytic assay

In order to perform the safety evaluation of the most potent complex $Cs^+[Eu((+)\text{–tfac})_4]^-$, the hemolytic activity was performed in human red blood cells. The experiment was conducted by incubating erythrocyte suspension (4%) in phosphate buffered saline (PBS) with the compound at 25 and 50 μM concentrations at 37 °C for 1 h in triplicate. Triton X-100 (0.1%) was used as the positive control and PBS as the negative control. After proper incubation, the supernatant was collected, and absorbance was measured at 405 nm. The hemolysis percentage was calculated using the followed equation:

$$\text{Hemolysis (\%)} = (\text{O.D. Compound} - \text{O.D. Negative control})/(\text{O.D. Positive control} - \text{O.D. Negative control}) \times 100.$$

Results and discussion

The synthesis of the complexes was carried out by following a reported procedure with slight modifications (Fig. S1, ESI†).[24,25] Four sets of Eu(II) complexes with the molecular formula $M^+[Eu((+)\text{–tfac})_4]^-$ (M = Cs, Rb, K, Na) were synthesized by varying the alkali metal ion (Fig. 2a). The Europium complex $Cs^+[Eu((+)\text{–tfac})_4]^-$ was structurally authenticated by single crystal X-ray diffraction, and the corresponding crystallographic data are listed in Table S1 (ESI†). Unlike the previously reported Eu(III) complex with the heptafluorobutyryl camphorate ligand, the Eu center in $Cs^+[Eu((+)tfac)_4]^-$ adopts a ten-coordinated bicapped structure (Fig. 2b and Fig. S2, ESI†). Eu(III) is chelated to eight oxygen atoms from the four bidentate ligands. In addition to this, a water molecule coordinates to Eu(III) on opposite sides forming a bridge between Eu and Cs. The Eu–O bond lengths are in the range of 0.23–0.24 nm for coordination to the ligands and around 0.21 nm for coordination to water. The Cs^+ in $Cs^+[Eu((+)\text{-tfac})_4]^-$ coordinates to one C–F bond in each of the four $-CF_3$ groups, resulting in a strong $M^+\cdots FC$ electrostatic interaction. In addition to this, the Cs^+ interacts with oxygen atoms of the ligand through coordinate bonds. These interactions span within 0.35 nm, slightly higher than what is reported on similar lanthanide complexes.[24] The steric effects from the bulky camphor system are outweighed by the presence of the exceptional $M^+\cdots FC$ interactions resulting in rigid chiral orientation. The presence of coordinate bonds on

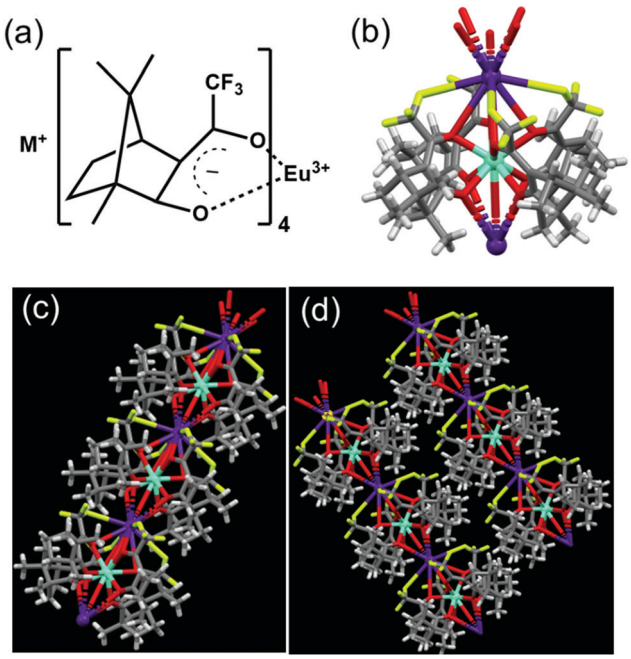

Fig. 2 (a) Molecular structure of $M^+[Eu((+)–tfac)_4]^-$ (M = Na, K, Rb, Cs). (b–d) X-ray crystal structure of (b) the $Cs^+[Eu((+)–tfac)_4]^-$ complex, (c) its one-dimensional array and (d) the network structures.

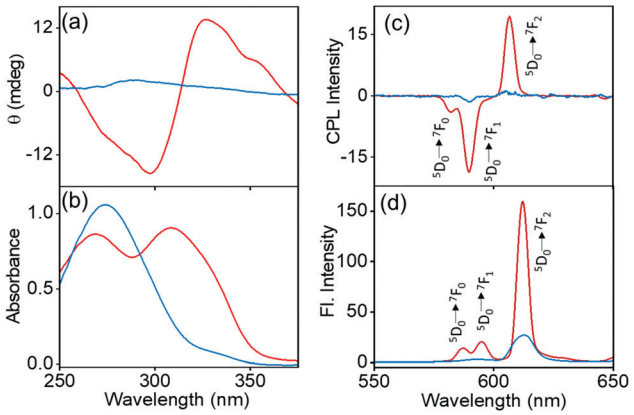

Fig. 3 (a) CD, (b) absorption, (c) CPL and (d) luminescence spectra of $Cs^+[Eu((+)\text{-}tfac)_4]^-$ (red traces) and $Rb^+[Eu((+)\text{-}tfac)_4]^-$ (blue traces) in chloroform (concentration = 2.0 mM; excitation wavelength λ_{ex} = 352 nm).

the $Cs^+[Eu((+)\text{-}tfac)_4]^-$ complex leads to the formation of an interesting one-dimensional polymer crystal (Fig. 2c and Fig. S2c, ESI†). The five coordinate bonds facilitate the formation of such a polymer network. Further extension of the network leads to arrays of the crystals resulting in coordination network structures as evident from Fig. 2d and Fig. S2d (ESI†). The arrays of networks are held together by weak van der Waals interactions. Such an unusual arrangement of the ligands around the metal center is expected to influence the properties of the complex, and further insights in this regard are established through the photophysical and chiroptical investigations of the complexes.

To analyse the preliminary photophysical characteristics of the synthesized Eu(III) complexes, chloroform was selected as the solvent wherein the complexes remain dispersed in their monomeric state.[20] The CD spectra of the $Cs^+[Eu((+)–tfac)_4]^-$ complex exhibited bisignate signals at the corresponding absorption peak at around 310 nm (Fig. 3a and b). The bisignate peak arises due to the exciton coupling between the long-axis π–π* transition dipole moments of the (+)–tfac ligands around the Eu(III) ion indicating a chiral orientation between the ligands. Surprisingly, other complexes (Rb, K and Na) under similar conditions exhibited a weak positive CD indicating the disruption of configurational chirality on decreasing the size of the alkali metal ion (Fig. 3a, b and Fig. S3, ESI†). Such an observation is suggestive of the dissociation of the tetrakis(+)–tfac Eu(III) complex into the tris derivative, $[Eu((+)–tfac)_3]$.[25,38] The presence of $[Eu((+)–tfac)_3]$ was independently verified by collecting the CD spectra of the complex in chloroform (Fig. S4, ESI†). The CD profile resembled that of $M^+[Eu((+)–tfac)_4]^-$ (M = Rb, K, Na) confirming the dissociation of the tetrakis(+)–tfac Eu(III) complex with the decrease in the size of the metal ion. The emission spectra of the Cs complex showed spectral features typical of similar europium complexes: peaks at 595 and 610 nm corresponding to the $^5D_0 \rightarrow {}^7F_1$ and $^5D_0 \rightarrow {}^7F_2$ transitions, respectively (Fig. 3d). Intense CPL was observed at both emission wavelengths. The extent of chiral dissymmetry which is quantified using the anisotropic factor can be calculated as $g_{lum} = 2(I_L - I_R)/(I_L + I_R)$, where I_L and I_R are the intensities of left- and right-circularly polarized light, respectively.[39–41] While the electric dipole allowed transition at 610 nm exhibited a low g_{lum} value of 0.128, a high g_{lum} value of −0.701 was observed for the $^5D_0 \rightarrow {}^7F_1$ transition at 595 nm, which is well-suited for CPL studies as it satisfies the selection rule for magnetic-dipole, $\Delta J = 0, \pm 1$ (except $0 \leftrightarrow 0$) (Fig. 3c). The high anisotropy in luminescence can be attributed to the helical arrangement of the tfac around the metal center. Moreover, the peculiar structural features of the complex provide it a favourable geometry that contributes to the high anisotropic factor as evident from the crystal structure.

The spectral features showed a radical change on changing the alkali metal ion in the complexes. A drastic decrease in the CPL peak intensity was observed on decreasing the size of the alkali metal ion. The existence of a dynamic equilibrium between the complexed state $M^+[Eu((+)–tfac)_4]^-$ and the dissociated state $Eu((+)–tfac)_3$ is responsible for the observed spectral features.[25] The nature of equilibrium depends largely on the size of the alkali metal ion. Unlike the heptafluoro derivative,[25] the lower number of fluorine atoms in the trifluoro analogue causes the equilibrium to shift towards the dissociated state with a small change in the size of the metal ion. The dissociated complex $Eu((+)–tfac)_3$ exhibited very low luminescence and a weak chirality in chloroform (Fig. S4, ESI†). This in turn resulted in a decrease in the overall dissymmetry factor for the complexes formed using Rb^+, K^+ and Na^+ as metal ions (Fig. S3c and d, ESI†). The existence of such an equilibrium was further confirmed with the help of concentration dependent CPL measurements (Fig. S5, ESI†). The concentration dependent studies in chloroform showed major changes in the g_{lum}

value only in the case of the Cs complex. The g_{lum} for the $^5D_0 \rightarrow {}^7F_1$ transition in $Cs^+[Eu((+)\text{–}tfac)_4]^-$ decreased from −0.701 to −0.513 upon lowering the concentration to 1.0 mM (Table S2, ESI†). A similar change was noticed for the $^5D_0 \rightarrow {}^7F_2$ transition as well. The Cs complex that remained majorly in the undissociated form at higher concentration (2.0 mM) experienced a shift in equilibrium towards the dissociated $Eu((+)\text{–}tfac)_3$ state upon decreasing the concentration (1.0 mM). Such an equilibrium shift resulted in a decrease in the luminescence anisotropy value. In contrast, the effect of concentration on the other derivatives (Rb, K and Na) was minimal as these complexes remained in the dissociated state even at a higher concentration of 2.0 mM. The dissociation equilibrium would undergo minimal changes upon further dilution. The luminescence lifetime of the $Cs^+[Eu((+)\text{–}tfac)_4]^-$ complex exhibited a monoexponential decay with an excited state lifetime of 0.63 ms (Table 1). In contrast, the Rb analogue exhibited a triexponential decay with lifetimes of 0.63, 0.016 and 0.027 ms, further confirming the presence of multiple emitting species in solution (Fig. S6, ESI†). An attractive feature of the $Cs^+[Eu((+)\text{–}tfac)_4]^-$ complex is its high luminescence quantum yield. A remarkably high quantum yield of 20.3% was observed for the 2.0 mM solution of the complex in chloroform. However, the values were quite low (below 2.0%) for Rb, K and Na derivatives owing to the weakly emissive nature of the dissociated tris derivative $Eu((+)\text{–}tfac)_3$.

For any system to be developed for practical applications, it is necessary that its properties are demonstrated in the solid state. To investigate the properties of the complexes in the solid state, the complexes were embedded in a polymer matrix. This was achieved by preparing PMMA (8 wt%) films of the complexes in chloroform. The hybrid films retained the properties in the solid state and exhibited spectral features similar to that observed in solution. The solid-state CD measurements revealed a bisignate peak for the Cs derivative, whereas weak positive peaks were observed for the other derivatives (Fig. S7, ESI†). The Cs derivative exhibited an intense CPL signal with a high g_{lum} value of −0.29 for the $^5D_0 \rightarrow {}^7F_1$ transition corresponding to the magnetic dipole allowed band at 595 nm (red trace in Fig. 4a and b). Analogous to the observations in chloroform solution, the g_{lum} values in films decreased with the decreasing size of the alkali metal ion (Fig. S8, ESI†), with the CPL almost disappearing for the Na derivative (green trace in Fig. 4a and b). A low value of −0.092, −0.089 and −0.003 was observed for the Rb, K and Na analogues, respectively. As the polymer films were prepared from complexes dispersed in chloroform, the chiral anisotropy of complexes followed a similar trend as in chloroform; the Cs derivative exhibited a high g_{lum} value and a sudden decrease was observed upon decreasing the size of the metal ion to Rb, K and Na. This is due to the existence of higher proportion of the undissociated complex in $Cs^+[Eu((+)\text{-}tfac)_4]^-$ and the shift in equilibrium towards the dissociated species $Eu((+)\text{–}tfac)_3$ for other derivatives (Rb, K and Na). This effect could be further established by preparing films using solution at two different concentrations (Fig. S9, ESI†). Upon decreasing the concentration of the complex, a decrease in the g_{lum} value was observed, the effect being prominent for the Cs derivative and minimal for the other complexes (Table S3, ESI†) (*vide supra*). While the trend followed solution state investigations, the absolute values diminished in the solid state. The difference in luminescence and CPL activity in solid state can be attributed to various factors such as the crystal packing and the solvation effects.[42,43] A lower value in the solid KBr pellet has been reported on similar systems and this could be due to the unfavourable orientations and the lower stability of the complexes in the matrix.[44] The complexes were stable to measurements in solution; however, longer exposure of the same point on the film during larger accumulations led to a decrease in luminescence as well as CPL intensity of the samples. While the g_{lum} values decreased in solid films, the value observed for the complex $Cs^+[Eu((+)\text{–}tfac)_4]^-$ was high enough for any practical application.

Chiral measurements on solid surfaces are prone to artefacts due to linear dichroism/linear birefringence. To establish

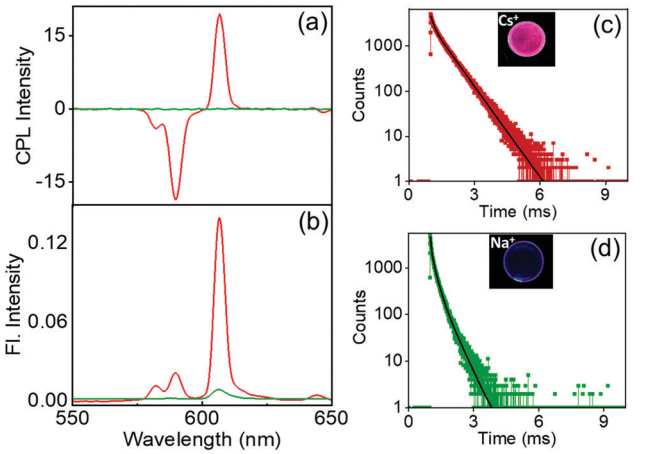

Fig. 4 (a) CPL and (b) fluorescence spectra of $Cs^+[Eu((+)\text{–}tfac)_4]^-$ (red traces) and $Na^+[Eu((+)\text{–}tfac)_4]^-$ (green traces) embedded in the PMMA films. (c and d) Luminescence lifetime plots of the hybrid PPMA films composed of (c) $Cs^+[Eu((+)\text{–}tfac)_4]^-$ and (d) $Na^+[Eu((+)\text{–}tfac)_4]^-$ (λ_{ex} = 352 nm). The inset shows the photographs of the corresponding films collected upon excitation using a 365 nm UV lamp.

Table 1 The luminescence lifetime data of the complexes $M^+[Eu((+)\text{–}tfac)_4]^-$ (M = Cs, Rb, K, Na) in chloroform, PMMA film and in DMSO

Chloroform		PMMA films		DMSO	
M	τ (ms)	M	τ (ms)	M	τ (ms)
Cs	0.63 (100%)	Cs	0.65 (88.8%) 0.13 (11.2%)	Cs	0.13 (65.6%) 0.44 (34.4%)
Rb	0.63 (92.1%) 0.016 (5.9%) 0.027 (2.0%)	Rb	0.40 (66.3%) 0.16 (33.7%)	Rb	0.18 (54.6%) 0.02 (44.4%)
K	—	K	0.37 (63.5%) 0.09 (36.5%)	K	0.18 (91.9%) 0.07 (8.1%)
Na	—	Na	0.34 (65.3%) 0.08 (34.7%)	Na	0.15 (78.5%) 0.51 (15.1%) 0.02 (6.4%)

the uniformity of data, the CPL and CD spectra were collected from multiple points by rotating and flipping the films (Fig. S10 and S11, ESI†). Except for slight variations in the intensity of the peaks, the sign as well as the g_{lum} values of the peaks was consistent ruling out the possibility of any artefacts due to linear polarization effects (Table S4, ESI†). Hence, the repeated measurements prove the reproducibility of the dissymmetry factor of the complexes in the solid-state beyond doubt. The complexes in polymer films exhibit bright luminescence upon excitation using UV light highlighting the potential of these complexes to be developed as light-emitting materials (Fig. S12a, ESI†). The lifetime plots showed biexponential decay for the Cs derivative. The major and minor species exhibited lifetimes of 0.65 ms (88.8%) and 0.13 ms (11.2%) respectively (Fig. 4c). The other derivatives also exhibited biexponential curves (Fig. 4d and Fig. S8c, d, ESI†); however, both emitting species were predominant, indicating a shift in the dissociation equilibrium with the decrease in the size of the alkali metal ion (Table 1).

Self-assembly of molecular systems is a facile approach that can be adopted for the fabrication of robust nanomaterials.[45] Self-assembly of chiral molecules can result in chiral nanostructures that can function as optically active materials for application in diverse fields.[46] To investigate the self-assembly of the $M^+[Eu((+)\text{-tfac})_4]^-$ complexes, the compounds were dispersed in DMSO. The morphological features of the as-dispersed complexes were studied using scanning microscopy (SEM) and transmission electron microscopy (TEM). SEM images of samples drop cast on silicon wafer showed well defined structures. Long wire like structures were observed from $Cs^+[Eu((+)\text{–tfac})_4]^-$ and $Na^+[Eu((+)\text{–tfac})_4]^-$ (Fig. 5a and b). Similar morphological features were observed for the nanostructures formed from different complexes (Fig. S13, ESI†). Further characterization using TEM imaging confirmed the morphology of the self-assembled nanostructures (Fig. 5c–e). Long wire like structures with an average width of 200 nm and length of few micrometers were observed in all the cases.

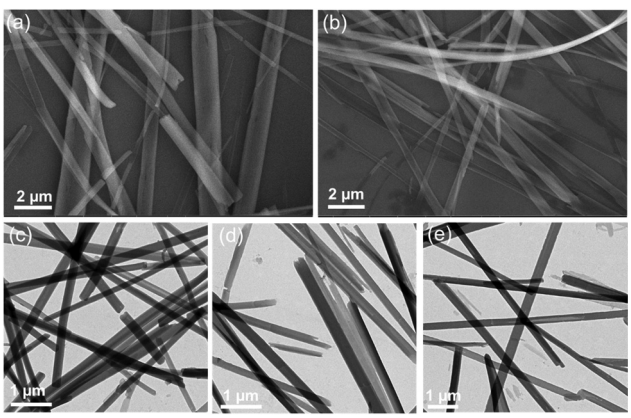

Fig. 5 SEM images of nanostructures formed in DMSO solutions of (a) $Cs^+[Eu((+)\text{–tfac})_4]^-$ and (b) $Na^+[Eu((+)\text{–tfac})_4]^-$. TEM images of the self-assembled aggregates formed from (c) $Cs^+[Eu((+)\text{–tfac})_4]^-$, (d) $Rb^+[Eu((+)\text{–tfac})_4]^-$ and (e) $K^+[Eu((+)\text{–tfac})_4]^-$.

With the complexes being chiral in nature, the assembled structures are also expected to be chiral. Close analysis of the images revealed that the wired structures exhibited a helical twist in certain regions, even though the twist was not apparent from the images. The images confirm that the complexes self-assemble to form well defined aggregated structures in suitably selected solvents.

Investigation of the luminescence properties of the nanostructures is vital to finding potential applications for the materials. The luminescence spectra of the complexes exhibited typical spectral signatures observed for similar Eu complexes: an intense peak at 610 nm corresponding to the electric dipole transitions ($^5D_0 \rightarrow {}^7F_2$) and a weaker peak at 591 nm attributed to the magnetic dipole allowed transitions ($^5D_0 \rightarrow {}^7F_1$). Additional peaks with weaker intensities corresponding to various transitions in lanthanides were also observed. The fluorescence intensity increased with an increase in the size of the alkali metal ion; the most intense peak was observed for the Cs derivative, the peak intensity gradually decreased for the Rb and K analogues, and a weak peak was observed for the Na derivative (Fig. 6a). The excited state chiral properties of the complexes were explored using CPL spectroscopy. The CPL spectra of the complexes exhibited peaks in the fluorescence range. The peak observed at 610 nm showed maximum intensity in CPL; however, the g_{lum} values were found to be modest at around 0.133 for $Cs^+[Eu((+)\text{-tfac})_4]^-$. In contrast, the peak at 591 nm exhibited a significantly high g_{lum} value (Fig. 6b). The chiral luminescence anisotropy varied depending on the alkali metal ion. A high g_{lum} of −0.691 was observed for $Cs^+[Eu((+)\text{-tfac})_4]^-$, and the value decreased to −0.565, −0.492, and

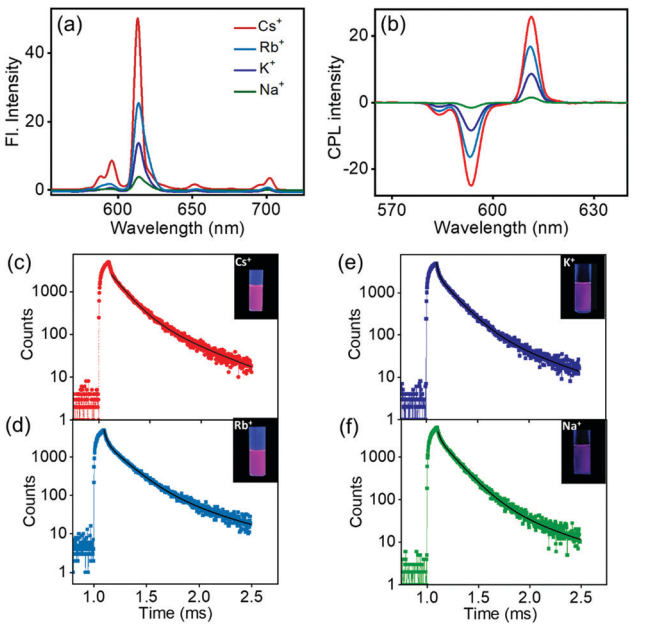

Fig. 6 (a) Fluorescence and (b) CPL spectra of the nanostructures formed from $M^+[Eu((+)\text{–tfac})_4]^-$ complexes in DMSO (concentration = 2.0 mM; λ_{ex} = 371 nm). The excited state lifetime plots of (c) $Cs^+[Eu((+)\text{–tfac})_4]^-$, (d) $Rb^+[Eu((+)\text{–tfac})_4]^-$, (e) $K^+[Eu((+)\text{–tfac})_4]^-$ and (f) $Na^+[Eu((+)\text{–tfac})_4]^-$. The insets show the photographs of the DMSO solutions of the corresponding samples collected upon excitation using a 365 nm UV lamp.

−0.440 for $Rb^+[Eu((+)\text{-tfac})_4]^-$, $K^+[Eu((+)\text{-tfac})_4]^-$ and $Na^+[Eu((+)\text{-tfac})_4]^-$ complexes respectively, for the magnetic dipole allowed $^5D_0 \rightarrow {}^7F_1$ transition at 591 nm. The remarkable g_{lum} values are the result of multiple factors; the assembly of the complexes contributes to the enhanced chiral anisotropy in addition to the rigid chiral orientation facilitated by the stereochemical lock offered by the alkali metal ions as observed in the XRD data (*vide supra*). In contrast to the observations in chloroform, the concentration dependent studies in DMSO showed changes in g_{lum} values for all complexes (Fig. S14, ESI†). A decrease in chiral anisotropy upon decreasing the concentration indicates a shift in equilibrium towards the dissociated tris derivative $Eu((+)\text{–tfac})_3$ upon lowering the concentration in all the four derivatives (Table S5, ESI†). The complexes remained majorly in the undissociated form at higher concentration (2.0 mM) and a shift towards the dissociated form was observed upon decreasing the concentration (1.0 mM). The highly luminescent nanomaterials have great potential to be used in various applications (Fig. S12b, ESI†). Due to the non-availability of the ligand possessing opposite chirality, we could not obtain mirror image CPL plots for the complexes with opposite signals.

The excited state lifetime data of the nanostructures were collected in DMSO. The $Cs^+[Eu((+)\text{-tfac})_4]^-$ complex showed a biexponential decay with excited state lifetimes of 0.13 and 0.44 ms (Fig. 6c). The Rb derivative exhibited similar decay curves with lifetime values of 0.18 and 0.02 ms (Fig. 6d). A similar trend was observed in the case of the K and Na derivatives (Fig. 6e and f). A shift in the lifetime of the major emitting species was observed in all cases indicating that the luminescence originates from the aggregated structures for all four complexes in DMSO (Table 1). This change can be attributed to the shift in emission from the complexes in chloroform to the self-assembled aggregates in DMSO. Moreover, the presence of multiple emitting species is quite common in such self-assembled aggregated structures.[20]

A comparison of the photophysical properties of the complexes in chloroform and DMSO shows certain notable differences. In chloroform, the Cs derivative exhibited high luminescence quantum yield and CPL anisotropy. A sudden decrease in both luminescence and CPL could be observed on moving from Cs to Rb complex indicating the role of the size of the alkali metal ion in holding the complex in its preferred chiral geometry. The tetrakis(+)–tfac Eu(III) complex dissociates into the tris derivative leading to low luminescence as well as CPL activity upon decreasing the size of the alkali metal ion. In contrast the variation in g_{lum} values was gradual in DMSO. The $Cs^+[Eu((+)\text{-tfac})_4]^-$ complex exhibited high chiral anisotropy, which gradually decreased in the order Cs > Rb > K > Na (Table 2). The lowering of chiral anisotropy with the size of the alkali metal ion is evident in DMSO as well; however, the aggregated structures might hold the complexes in their preferred chiral orientation leading to reasonably high g_{lum} values even with smaller alkali metal ions. From these observations, it can be concluded that the effect of self-assembly on the g_{lum} value was less prominent in $Cs^+[Eu((+)\text{-tfac})_4]^-$ where the size of the alkali metal ion is large. Hence, the $Cs^+[Eu((+)\text{-tfac})_4]^-$ complexes exhibited almost similar g_{lum} values in both chloroform and DMSO. The values were found to decrease upon decreasing concentration in both cases. In contrast, the effect of self-assembly was prominent in complexes with smaller size of the alkali metal ion (Rb, K and Na). In all three derivatives, the g_{lum} value was found to be very low in chloroform. However, these complexes exhibited a high value in DMSO wherein aggregation was observed. Hence, these complexes remain in the dissociated form in chloroform and the equilibrium shifts more towards the undissociated form in DMSO. Even though the equilibrium is shifted more towards the undissociated complex, the presence of $Eu((+)\text{–tfac})_3$ in the aggregates cannot be completely ruled out. This was established through concentration dependent studies where all four complexes showed a gradual decrease in the g_{lum} values on lowering the concentration. This is an indication of the shift in equilibrium towards the dissociated form at lower concentrations. Even though an exact quantification of the dissociated species within the aggregates is difficult, CPL investigations indicate that their proportion in the aggregated structures is low.

Table 2 The g_{lum} values of the complexes in chloroform and the nanostructures in DMSO

Chloroform			DMSO		
M	g_{lum} ($^5D_0$–$^7F_1$)	g_{lum} ($^5D_0$–$^7F_2$)	M	g_{lum} ($^5D_0$–$^7F_1$)	g_{lum} ($^5D_0$–$^7F_2$)
Cs	−0.701	0.128	Cs	−0.691	0.133
Rb	−0.155	0.051	Rb	−0.565	0.054
K	−0.025	0.003	K	−0.492	0.047
Na	−0.005	0.001	Na	−0.440	0.041

For any application of the complexes and the nanostructures in the biological system, it is important that their properties are investigated in aqueous medium. The complexes being insoluble in water could not be dispersed in aqueous medium directly; instead the samples were prepared in a solution possessing high water content. For this, samples with varying water:DMSO composition were prepared and analysed for their CPL activity. CPL investigations revealed that the system is stable up to a high-water content of 80% (Fig. S15, ESI†). The stability of the samples indicates the potential of these systems to be used in biological applications.

Having established the good chiroptical properties of the Eu(III) complexes and the corresponding nanostructures, we further explored the potential of these materials in the biomedical field, which has been least explored. Indiscriminate use of antibiotics in medicine and agriculture has led to the creation of multidrug resistant microbes which is turning out to be a significant challenge in clinical settings globally. There is an urgent demand for new and effective molecular systems that can inhibit the growth of such microbes and combat the spread of bacterial infections. Karthikeyan *et al.* synthesized a chiral lanthanide complex with antibacterial properties, which was toxic against Gram positive *Staphylococcus aureus* and Gram negative *Escherichia coli*.[35] Antimicrobial activity is elucidated based on the release of Ln(III) ions into the cell that affects the metabolic synthesis of peptidoglycan thereby disrupting the osmotic stability of the bacterial cell wall causing structural modifications and cell death. We investigated the antibacterial activity of the synthesized heterobimetallic

europium complexes $M^{+}[Eu((+)\text{–tfac})_4]^{-}$ (M = K, Rb and Cs) against a set of clinical and multidrug-resistant strains of Gram positive pathogens (*Staphylococcus aureus* and *Enterococcus faecalis*) and Gram negative pathogens (*E. coli*, *Pseudomonas aeruginosa*, *Salmonella typhi* and *Vibrio cholera*).

Initial studies were carried out to analyse the antibacterial activity of $Cs^{+}[Eu((+)\text{-tfac})_4]^{-}$ with the selected set of Gram positive and Gram negative pathogens. The complex exhibited potent inhibitory activity only against Gram positive pathogens – *S. aureus*, MRSA, and *E. faecalis* isolates – whereas moderate activity was observed against *E. coli* and *S. typhi*. The complex did not show much activity against *V. cholerae* MCV09 and *P. aeruginosa* ATCC 27853. The Cs derivative exhibited 88% inhibition against *S. aureus* strains and 78% inhibition against *E. faecalis* strains at 25 μM concentration. The same complex exhibited 52% inhibition against *E. coli*, 41% inhibition against *S. typhi*, 29.5% inhibition against *V. cholerae* and 27% inhibition against *P. aeruginosa* at 35 μM concentration. Reduced activity was observed at lower concentrations (Fig. 7a). Further, the MIC value was determined to be 15 and 20 μM against *S. aureus* and *E. faecalis* isolates, respectively. The observed results could be explained by examining the cell wall composition of bacteria. Gram negative bacteria have an extra outer membrane made of lipoproteins which hinders the penetration of administered drugs.[47] One major factor aiding the antibacterial property of lanthanide ions is their size. Due to their similarity in size with the Ca^{2+} ion, and higher charge affinity, they can easily replace Ca^{2+} ions in many enzymes and proteins leading to inhibition of cell activities and eventually cell death.[48] Moreover, the lipophilic nature of the Ln(III) complexes enhances their penetration across the lipid membrane of the cell, affecting the development and growth of bacterial cells.[49]

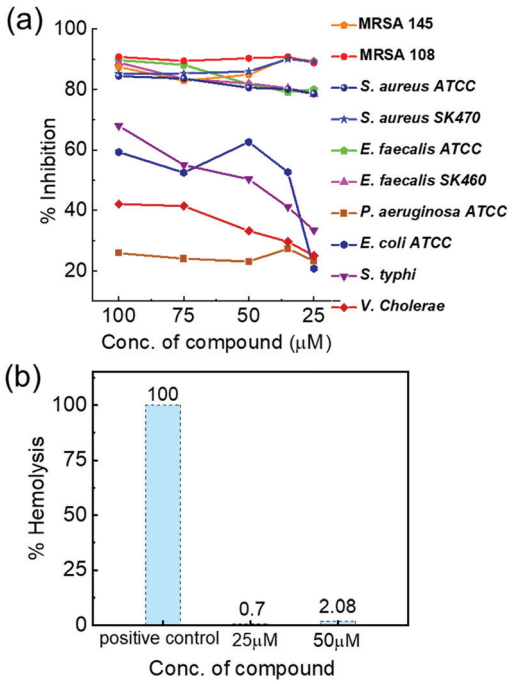

Fig. 7 (a) Percentage inhibition of the $Cs^{+}[Eu((+)\text{-tfac})_4]^{-}$ complex against major Gram positive and Gram negative pathogens. (b) Haemolytic activity of the compound on human erythrocytes after 1 h of incubation at 37 °C.

To understand the role of the size and charge of the alkali metal ion that coordinates to $Eu((+)\text{–tfac})_3$ in the antibacterial activity, we carried out similar experiments with other complexes containing Rb^{+} and K^{+} ions. $Rb^{+}[Eu((+)\text{–tfac})_4]^{-}$ and $K^{+}[Eu((+)\text{–tfac})_4]^{-}$ complexes also showed high antibacterial activity against Gram positive pathogens (Fig. S16 and S17, ESI†). The complexes were highly selective to *S. aureus*, MRSA and *E. faecalis* pathogens and feebly active against Gram negative pathogens. These complexes exhibited around 70–75% inhibition compared to the 88% inhibition showed by $Cs^{+}[Eu((+)\text{–tfac})_4]^{-}$ against *S. aureus*. Thus, the results clearly indicate a highly potent inhibitory activity for all the three derivatives. These observations can be explained temporally in terms of hard–soft theory developed by Pearson.[50] The surface of a bacterial cell contains soft ions like phosphoric acid and carboxyl groups which can complex selectively with larger cations and thus allow their facile penetration into the cell. Bacteria such as *S. aureus* have been listed under highly resistant pathogens by the WHO, and hence, the development of effective antibacterial agents against such pathogens is extremely important in tackling related ailments. Studies could not be extended to $Na^{+}[Eu((+)\text{-tfac})_4]^{-}$ due to the low solubility. Finally, the hemolytic activity of the most potent complex $Cs^{+}[Eu((+)\text{–tfac})_4]^{-}$ was evaluated towards human red blood cells. A hemolytic activity of 0.7 and 2.08% was observed at 25 and 50 μM concentrations, respectively (Fig. 7b). Hemolytic activity below 10% is commonly recognized as a safe cut-off.[51] Hence, the complex $Cs^{+}[Eu((+)\text{-tfac})_4]^{-}$ is found to be non-hemolytic and can be considered safe for humans.

Conclusions

In summary, we have synthesized a set of Eu(III) complexes that exhibit high luminescence quantum yield and CPL dissymmetry both in the solution state and in solid films. The single-crystal X-ray diffraction of the $Cs^{+}[Eu((+)\text{–tfac})_4]^{-}$ complex revealed a novel crystalline structure. The complexes on self-assembly formed chiral nanostructures that exhibited remarkably high CPL activity, making these materials potential candidates for application in chiral optical devices. The most exciting feature with the complexes is their high antibacterial activity towards Gram positive multidrug resistant strains *Staphylococcus aureus* and *Enterococcus faecalis*, some of which have been enlisted by the WHO as highly multidrug resistant pathogens. Identification and characterization of such novel molecules with application in infectious disease treatment is the need of the hour. Hence, the developed molecules and materials hold great prospects for future applications in diverse fields, ranging from antimicrobial agents to security inks, bioimaging agents and circularly polarized OLEDs.

Conflicts of interest

There are no conflicts to declare.

Acknowledgements

J. K. acknowledges financial support from the Department of Science and Technology-SERB (DST-SERB), Government of India, under the Core Research Grant (DST-SERB project: CRG/2019/002715). B. M. acknowledges the fellowship and funding from DST, Government of India under the woman scientist program [SR/WOS-A/CS-22/2017(G)]. K. S. acknowledges CSIR, Government of India, for the research associateship. A. M. L. acknowledge DST-INSPIRE and A. S. acknowledges IISER Tirupati for the fellowship. K. S. and S. T. are thankful to the Director, RGCB, for the facilities provided. The authors acknowledge IISER Tirupati for providing the research facilities. The authors thank Prof. K. George Thomas and Mr Sanoop M. S., IISER Thiruvananthapuram, for their generous help with SEM imaging.

Notes and references

1 J. Kumar, K. G. Thomas and L. M. Liz-Marzan, *Chem. Commun.*, 2016, **52**, 12555–12569.
2 Y. Sang, J. Han, T. Zhao, P. Duan and M. Liu, *Adv. Mater.*, 2019, **32**, 1900110.
3 N. Berova, L. Di Bari and G. Pescitelli, *Chem. Soc. Rev.*, 2007, **36**, 914–931.
4 R. Thomas, J. Kumar, J. George, M. Shanthil, G. N. Naidu, R. S. Swathi and K. G. Thomas, *J. Phys. Chem. Lett.*, 2018, **9**, 919–932.
5 F. S. Richardson and J. P. Riehl, *Chem. Rev.*, 1977, **77**, 773–792.
6 J. Han, S. Guo, H. Lu, S. Liu, Q. Zhao and W. Huang, *Adv. Opt. Mater.*, 2018, **6**, 1800538.
7 P. Kumar, S. Singh and B. K. Gupta, *Nanoscale*, 2016, **8**, 14297–14340.
8 K. Dhbaibi, P. Matozzo, L. Abella, M. Jean, N. Vanthuyne, J. Autschbach, L. Favereau and J. Crassous, *Chem. Commun.*, 2021, **57**, 10743–10746.
9 S. Maniappan, A. B. Jadhav and J. Kumar, *Front. Chem.*, 2021, **8**, 968.
10 K. Ma, W. Chen, T. Jiao, X. Jin, Y. Sang, D. Yang, J. Zhou, M. Liu and P. Duan, *Chem. Sci.*, 2019, **10**, 6821–6827.
11 J. Kumar, T. Nakashima and T. Kawai, *J. Phys. Chem. Lett.*, 2015, **6**, 3445–3452.
12 F. Zinna and L. Di Bari, *Chirality*, 2015, **27**, 1–13.
13 R. Carr, N. H. Evans and D. Parker, *Chem. Soc. Rev.*, 2012, **41**, 7673–7686.
14 F. Zinna, L. Arrico, T. Funaioli, L. D. Bari, M. Pasini, C. Botta and U. Giovanella, *J. Mater. Chem. C*, 2022, **10**, 463–468.
15 J. Yuasa, T. Ohno, H. Tsumatori, R. Shiba, H. Kamikubo, M. Kataoka, Y. Hasegawa and T. Kawai, *Chem. Commun.*, 2013, **49**, 4604–4606.
16 J. C. G. Bunzli and S. V. Eliseeva, *Chem. Sci.*, 2013, **4**, 1939–1949.
17 D. E. Barry, D. F. Caffrey and T. Gunnlaugsson, *Chem. Soc. Rev.*, 2016, **45**, 3244–3274.
18 E. G. Moore, A. P. S. Samuel and K. N. Raymond, *Acc. Chem. Res.*, 2009, **42**, 542–552.
19 J. Zhang, Y. Zhou, Y. Yao, Z. Cheng, T. Gao, H. Li and P. Yan, *J. Mater. Chem. C*, 2020, **8**, 6788–6796.
20 J. Kumar, B. Marydasan, T. Nakashima, T. Kawai and J. Yuasa, *Chem. Commun.*, 2016, **52**, 9885–9888.
21 Y. B. Tan, Y. Okayasu, S. Katao, Y. Nishikawa, F. Asanoma, M. Yamada, J. Yuasa and T. Kawai, *J. Am. Chem. Soc.*, 2020, **142**, 17653–17661.
22 S. Wada, Y. Kitagawa, T. Nakanishi, M. Gon, K. Tanaka, K. Fushimi, Y. Chujo and Y. Hasegawa, *Sci. Rep.*, 2018, **8**, 16395.
23 T. Harada, H. Tsumatori, K. Nishiyama, J. Yuasa, Y. Hasegawa and T. Kawai, *Inorg. Chem.*, 2012, **51**, 6476–6485.
24 D. Shirotani, T. Suzuki and S. Kaizaki, *Inorg. Chem.*, 2006, **45**, 6111–6113.
25 J. L. Lunkley, D. Shirotani, K. Yamanari, S. Kaizaki and G. Muller, *J. Am. Chem. Soc.*, 2008, **130**, 13814–13815.
26 F. Song, Z. Zhao, Z. Liu, J. W. Y. Lam and B. Z. Tang, *J. Mater. Chem. C*, 2020, **8**, 3284–3301.
27 J. Y. R. Silva, L. L. da Luz, F. G. M. Mauricio, I. B. V. Alves, J. N. S. Ferro, E. Barreto, I. T. Waber, W. M. de Azevedo and S. A. Junior, *ACS Appl. Mater. Interfaces*, 2017, **9**, 16458–16465.
28 W. L. Chan, C. Xie, W.-S. Lo, J.-C. G. Bunzil, W.-K. Wong and K.-L. Wong, *Chem. Soc. Rev.*, 2021, **50**, 12189–12257.
29 X.-M. Chen, S. Zhang, X. Chen and Q. Li, *ChemPhotoChem*, 2022, **6**, e202100256.
30 L. Armelao, S. Quici, F. Barigelletti, G. Accorsi, G. Bottaro, M. Cavazzini and E. Tondello, *Coord. Chem. Rev.*, 2010, **254**, 487–505.
31 S. Zhang, W. Yin, Z. Yang, Y. Yang, Z. Li, S. Zhang, B. Zhang, F. Dong, J. Lv, B. Han, Z. Lei and H. Ma, *ACS Appl. Mater. Interfaces*, 2021, **13**, 5539–5550.
32 V. R. Carime, R. J. Katherine, C. L. Vincent, O. R. Marcelo, J. A. Sobrinho and A. de Bettencourt-Dias, *J. Med. Chem.*, 2021, **64**, 7724–7734.
33 G.-Y. Wu, X. Shi, H. Phan, H. Qu, Y.-X. Hu, G.-Q. Yin, X.-L. Zhao, X. Li, L. Xu, Q. Yu and H.-B. Yang, *Nat. Commun.*, 2020, **11**, 3178.
34 WHO publishes list of bacteria for which new antibiotics are urgently needed **https://www.who.int/news/item/27-02-2017-who-publishes-list-of-bacteria-for-which-new-antibiotics-are-urgently-needed** (accessed Jul 27, 2021).
35 G. Karthikeyan, K. Mohanraj, K. P. Elango and K. Girishkumar, *Transition Met. Chem.*, 2004, **29**, 86–90.
36 H. Wisplinghoff, T. Bischoff, S. M. Tallent, H. Seifert, R. P. Wenzel and M. B. Edmond, *Clin. Infect. Dis.*, 2004, **39**, 309–317.
37 R. Reik, F. C. Tenover, E. Klein and L. C. McDonald, *Diagn. Microbiol. Infect. Dis.*, 2008, **62**, 81–85.
38 J. L. Lunkley, D. Shirotani, K. Yamanari, S. Kaizaki and G. Muller, *Inorg. Chem.*, 2011, **50**, 12724–12732.
39 S. T. Duong and M. Fujiki, *Polym. Chem.*, 2017, **8**, 4673–4679.
40 Y. Deng, M. Wang, Y. Zhuang, S. Liu, W. Huang and Q. Zhao, *Light: Sci. Appl.*, 2021, **10**, 76.
41 Y. Nagata and T. Mori, *Front. Chem.*, 2020, **8**, 448.

42 H.-Y. Wong, W.-S. Lo, K.-H. Yim and G.-L. Law, *Chem*, 2019, **5**, 3058–3095.
43 F. Zinna, C. Resta, S. Abbate, E. Castiglioni, G. Longhi, P. Mineoe and L. D. Bari, *Chem. Commun.*, 2015, **51**, 11903–11906.
44 Y. Kondo, S. Suzuki, M. Watanabe, A. Kaneta, P. Albertini and K. Nagamori, *Front. Chem.*, 2020, **8**, 527.
45 X.-M. Chen, X.-F. Hou, H. K. Bisoyi, W.-J. Feng, Q. Cao, S. Huang, H. Yang, D. Chen and Q. Li, *Nat. Commun.*, 2021, **12**, 4993.
46 X.-M. Chen, Q. Cao, H. K. Bisoyi, M. Wang, H. Yang and Q. Li, *Angew. Chem., Int. Ed.*, 2020, **59**, 10493–10497.
47 Z. Breijyeh, B. Jubeh and R. Karaman, *Molecules*, 2020, **25**, 1340.
48 S. P. Fricker, *Chem. Soc. Rev.*, 2006, **35**, 524–533.
49 C. H. Evans, *Trends Biochem. Sci.*, 1983, **8**, 445–449.
50 R. S. Drago, *Inorg. Chem.*, 1973, **12**, 2211–2212.
51 K. Amin and R.-M. Dannenfelser, *J. Pharm. Sci.*, 2006, **95**, 1173–1176.